Sequence-Based Acoustic Noise Reduction of Clinical MRI Scans

Björn Heismann,[1,2]* Martin Ott,[3] and David Grodzki[1]

Purpose: Clinical MRI patients typically experience elevated acoustic noise levels of 80–110 dB(A). In this study, standard clinical turbo spin echo (TSE) and gradient echo (GRE) sequences were optimized for reduced acoustic noise at preserved diagnostic image quality.

Methods: The physical sources of acoustic noise generation in an MRI gradient coil were analyzed. A sequence conversion algorithm was derived that optimized the gradient time scheme for an arbitrary MRI sequence, preserving the governing spin physics. The algorithm was applied to generate "quiet" versions of standard clinical TSE and GRE sequences.

Results: The first volunteer images indicated that contrast-to-noise ratio and perceived diagnostic image quality remained on the same level for the algorithmic optimization. Additional careful TSE- and GRE-specific protocol adaptions yielded total acoustic noise reductions of up to 14.4 dB(A) for the TSE and up to 16.8 dB(A) for the GRE.

Conclusion: A physical sound pressure reduction of 81% (TSE) and 86% (GRE) for MRI patients was achieved. The results can be used to render MRI scans more patient-friendly in clinical practice, particularly for patients who are young, scared, or elderly. **Magn Reson Med 73:1104–1109, 2015.**

Key words: quiet MRI; acoustic noise reduction; algorithmic sequence optimization; spline interpolation; patient comfort

INTRODUCTION

In typical MRI examinations, the patient is exposed to high levels of acoustic noise. Depending on the scanner setup and sequence type, more than 110 dB(A) might be reached (1). These high acoustic noise levels are one of the main reasons for patient discomfort (2).

Acoustic noise in MRI is caused by several factors (1), with gradient activity being the most prominent. During typical MRI examinations, the gradient amplitude and polarity are switched in sub-milliseconds. Lorentz forces lead to mechanical vibrations of the gradient coil, which are coupled into the MRI system (3). The vibrations lead to sound pressure waves perceived as acoustic noise, with the patient bore serving as an acoustic membrane (4).

In the past decades, several approaches have been presented to minimize acoustic MRI noise associated with gradient activity (5–12). They can be grouped into hardware-based and sequence-based approaches.

Hardware solutions mainly aim to minimize the transfer of the mechanical gradient coil vibration to the rest of the system. Basic implementations include mechanical dampening and cover optimizations. Furthermore, the gradient coil can be sealed in a vacuum chamber (13). Additionally, active noise control systems were investigated (14,15). However, these approaches usually increase system complexity as well as cost, and in some cases they reduce patient bore size and effective gradient performance.

In sequence-based approaches, acoustic noise is reduced by optimizing the gradient activity and / or avoiding acoustic resonance frequencies. An optimization of gradient activity was employed by carefully modifying the gradient shapes to, for example, sinusoidal shapes (7) to minimize high acoustic frequencies and by reducing the applied gradient strength. Sequence-based approaches generally do not require any hardware changes.

In this study, we focused on a generic sequence-based approach that considered both the physics of acoustic noise generation and the conditions imposed by MR spin physics. As a practical result, a general-purpose sequence conversion algorithm was derived and applied to clinical turbo spin echo (TSE) and gradient echo (GRE) prototype sequences (including spoiled gradient recalled echo).

THEORY

Figure 1 shows the MR system setup and physical quantities related to the generation of acoustic noise. The gradient coil (GC) comprises three layers of independent coil setups. Each layer produces a dynamic gradient field component $G_j(t)$ in the spatial orthogonal directions $j=\{x,y,z\}$. The corresponding coil-driving currents $I_k(t)$ are generated by gradient amplifiers. The main field magnet provides the static field $\vec{B}_0$ in the patient z-axis direction.

The interaction between the magnetic field $\vec{B}$ and the transient electrical currents $\vec{I}$ generates Lorentz forces (16):

$$\vec{F} \propto \vec{I} \times \vec{B}. \quad [1]$$

Because the magnetic field is mostly directed in the z-direction and the GC currents I_φ are directed in the tangential φ direction (Fig. 1), radial Lorentz forces on the GC dominate. Axial and tangential force components are

[1]Siemens Healthcare, Magnetic Resonance Imaging, Erlangen, Germany.
[2]Friedrich-Alexander-University of Erlangen-Nuremberg, Pattern Recognition Lab, Erlangen, Germany.
[3]Research Center Magnetic-Resonance-Bavaria, Wuerzburg, Germany.
*Correspondence to: Björn Heismann, Siemens Healthcare Magnetic Resonance Imaging, Allee am Röthelheimpark 2, 91052 Erlangen, Deutschland. E-mail: bjoern.heismann@siemens.com, bjoern.heismann@gmx.de.
Received 2 December 2013; revised 6 February 2014; accepted 3 March 2014
DOI 10.1002/mrm.25229
Published online 29 May 2014 in Wiley Online Library (wileyonlinelibrary.com).

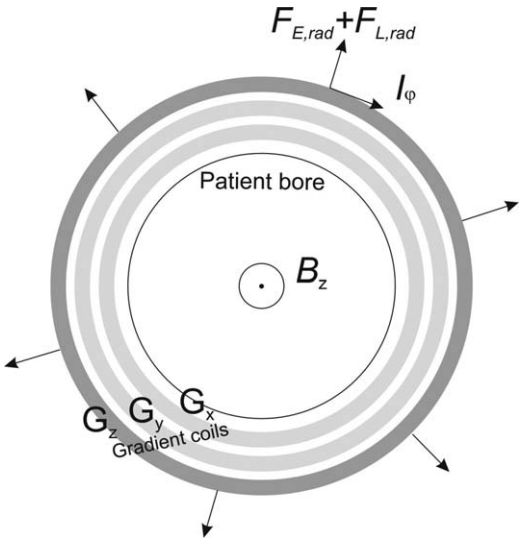

FIG. 1. MR system setup and quantities related to the generation of acoustic noise.

neglected in the following analytical approximation. We have the radial component

$$F_{L,rad} \propto I_\phi(t) \cdot B_z(t). \quad [2]$$

with the *z*-component of the magnetic field given by

$$B_z(t) = |\overrightarrow{B}_0| + \overrightarrow{r}\overrightarrow{G}(t) = B_0 + xG_x(t) + yG_y(t) + zG_z(t). \quad [3]$$

Because the tangential current component $I_{\varphi,k}$ of each gradient coil wiring layer k is proportional to the corresponding gradient field G_k and $B_Z \approx B_0$ as the fields created by the gradient coils are orders of magnitude smaller than the static field, Eqs. [2] and [3] lead to the linear approximation

$$F_{L,rad} = B_0\big(a_1 G_x(t) + a_2 G_y(t) + a_3 G_z(t)\big), \quad [4]$$

for the total radial Lorentz force on the GC with the system-specific constants a_1, a_2, a_3. This radial Lorentz force works against the GC's mechanical stiffness. Thus the elongation x is proportional to the radial Lorentz force. Because the sound pressure is approximately proportional to the velocity of the GC's surface, the resulting sound pressure is approximately proportional to the time derivative of the forces, $\rho \propto \dot{F}_{L,rad}$.

Eddy currents generated by time-varying magnetic fields are a second source of Lorentz forces on metallic surfaces in an MRI system. According to Maxwell's equations, eddy currents I_E are driven by a voltage proportional to the time-derivative of the magnetic flux and the Ohmic conductivity of the metallic surface (e.g., the conductors of the RF birdcage coil). We obtain

$$I_E \propto \frac{d}{dt}\phi \propto \frac{d}{dt}B. \quad [5]$$

The additional eddy current driven Lorentz force component on conductive metallic structures in the MRI is thus given by

$$F_E \propto \frac{d}{dt}B. \quad [6]$$

By substituting Eq. [3] and averaging over the GC's volume we obtain the approximation

$$F_E = B_0\big(b_1 \dot{G}_x(t) + b_2 \dot{G}_y(t) + b_3 \dot{G}_z(t)\big), \quad [7]$$

with the system-specific constants b_1, b_2, b_3. Note that the Lorentz force (Eq. [4]) is proportional to the transient gradient amplitudes, whereas the additional eddy current–driven Lorentz force (Eq. [7]) on conductive structures depends on the slew rates (i.e., the time derivatives of the gradient amplitudes). This creates a second-order derivate in the sound pressure for the eddy current–driven Lorentz force on metallic structures, further emphasizing higher frequency components.

The relative contribution of both sound pressure sources depends on the actual system setup. Metallic structures in the body coil, the local coil antennas, and the patient bed usually define the impact. For a standard MRI system, below a frequency of 100 Hz, the acoustic noise is usually dominated by the cold-head activity. Between 100 and 1000–1500 Hz, the noise generated by the radial Lorentz force is usually the main contribution (16). Beyond this range, the eddy current–driven Lorentz forces generally dominate.

For the scope of this paper, it is important to understand the connection of the force generation given by Eqs. [4] and [7] and the MRI sequence for typical sequence gradient building blocks.

In case of a section with constant gradient amplitude, the corresponding radial Lorentz force (Eq. [4]) is constant and the eddy current–driven Lorentz force (Eq. [7]) vanishes. As a result, no acoustic pressure wave is created in the MRI system. As a practical example, the radial ultra-short echo time sequence PETRA (17) uses mostly constant gradient amplitudes and exhibits practically no acoustic noise generation.

In the second case of a trapezoidal gradient shape with length T, the rising part $G(t) = SR \cdot t$ with slew rate SR leads to a linearly increasing radial Lorentz force and a constant eddy current–driven Lorentz force. In the decreasing part, $G(t) = G_{\max} - SR \cdot t$, creates a decreasing radial Lorentz force and a constant eddy current driven Lorentz force with opposite sign. An acoustic pressure wave results at the approximate frequency $f = 1/T$.

In standard clinical MRI sequences, the gradient fields and force generation are usually not optimized for scanning with low acoustic noise. The available high-gradient field amplitudes and slew rates of modern MRI gradient systems are leveraged to enable fast encoding or spoiling and well-defined spin conditions.

For the target of low acoustic noise "quiet" MRI, however, it is evident from both the formulas and the above examples that the gradient amplitudes, slew rates, and higher-order derivatives should be kept as low as possible. Natural constraints arise from the timing requirements of the sequence, imposed, for example, by the targeted echo time (TE) and repetition time (TR) and the associated clinical contrasts. This applies especially to the minimization of the gradient amplitudes. On the

other hand, slew rates and higher orders of time derivatives are usually less affected by this condition and should be minimized holistically over the complete MRI sequence.

In the k-space trajectory of the sequence given by

$$\vec{k}(t) = \gamma \int_0^t \vec{G}(t')dt'. \quad [8]$$

with the constant gyromagnetic ratio γ, the gradient amplitude $\vec{G}$ corresponds to a k-space velocity and the slew rate $\frac{d}{dt}\vec{G}(t)$ corresponds to a k-space acceleration. From this perspective, we need to control and minimize both k-space trajectory velocities and accelerations in MRI sequences. In k-space, this reflects rounded paths, especially between readout sections.

METHODS

For a practical and general-purpose implementation of the derived minimization criteria, we proposed an algorithm that converts a standard clinical MRI sequence into an optimized quiet sequence. The core idea of the algorithm relies on the fact that MRI sequences can be segmented into two alternating types of time intervals.

The first type of time interval, called KEEP, comprises radiofrequency (RF) pulse or readout activity. Gradient activities in KEEP intervals should be left unchanged, as they would interfere with RF spin signal generation or readout. Flow compensation gradient intervals also belong to this type.

The second type of time interval, called CHANGE, contains gradient activity that can be optimized over the whole time interval, as only the net spin phase change is relevant for the MR physics. In the following, t_1 and t_2 equal the time interval borders and G_{orig}(t) is the original gradient time curve. The new gradient curve $G_{newt}(t)$ shall fulfill five interval boundary conditions:

1,2) The altered gradient curve shall be continuous over the interval borders. This leads to $G_{new}(t_1) = G_{orig}(t_1)$, $G_{new}(t_2) = G_{orig}(t_2)$.

3,4) The gradient curve should be continuously differentiable to also keep the higher order derivatives small. We have d/dt $G_{new}(t_1) = 0$ and d/dt $G_{new}(t_2) = 0$, as the gradient curves are constant in the KEEP intervals.

5) The integral of the gradient curve from t_1 to t_2 shall equal the original sequence to preserve net spin phase changes, $\int_{t_1}^{t_2} G_{new}(t)dt = \int_{t_1}^{t_2} G_{orig}(t)dt$.

For each time interval of type CHANGE, these five requirements can be met by a fourth-order spline interpolation with five free parameters. As a procedure, the algorithm

a. takes the gradient, RF, and readout scheme of the sequence;
b. identifies the boundaries of type KEEP and CHANGE time intervals according to the RF and readout activity, as well as marked flow gradient pulses; and
c. performs a spline interpolation with the above boundary conditions for each CHANGE phase.

We tested the conversion algorithm on clinical-routine GRE and TSE sequences. In addition, we performed slight adaptions to the clinical protocol with the goal to reduce the slew rates further. These adjustments were chosen carefully to preserve the diagnostic content of the image. For the GRE sequence, a clinical T1 three-dimensional (3D) GRE head protocol with and without the conversion algorithm was tested using the following imaging parameters: TE = 4.92 ms; TR = 20 ms; flip angle = 25°; matrix = 512 × 512, field of view = 230 mm × 230 mm; acquisition time = 5:40 min; slice thickness = 0.9 mm. For the second step of optimization, a fast RF-pulse has been selected together with the conversion algorithm, while all other parameters were left unchanged. For the TSE sequence, a clinical T2 two-dimensional (2D) TSE head protocol with and without the conversion algorithm was tested using the following imaging parameters: TE = 99.5 ms; TR = 6000 ms; flip angle = 150°; matrix = 512×512, field of view = 220 mm × 220 mm; slice thickness = 4 mm; echo spacing = 9.0 ms; bandwidth = 220 Hz/pixel; acquisition time = 2:06 min. For the second step of optimization, the parameters TE = 104 ms, TR = 6100 ms, echo spacing = 10.4 ms, bandwidth = 250 Hz/pixel, and acquisition time = 2:08 min were used together with the conversion algorithm, while all other parameters were left unchanged.

In vivo volunteer scans were performed after informed consent on a MAGNETOM 3T Siemens scanner (Siemens Healthcare, Erlangen, Germany). The contrast-to-noise ratio (CNR) between tissue A and B was evaluated according to

$$CNR_{AB} = \frac{|Signal_A - Signal_B|}{SD}, \quad [9]$$

with the standard deviation measured in an object-free outer portion of the images. The acoustic noise levels were obtained with a 2238 Mediator sound level meter (Brueel & Kjaer GmbH, Bremen, Germany). The microphone was placed in the isocenter of the magnet at the averaged ear position of the patient. A water phantom was placed underneath the microphone. The acoustic spectrum was measured with a Brueel & Kjaer Pulse System (Brueel & Kjaer GmbH, Bremen, Germany).

RESULTS

Figure 2 shows a section of an original and an optimized clinical 3D GRE sequence to explain the main effects. First, the algorithm segments the sequence into KEEP and CHANGE intervals as described above. While gradients in the KEEP intervals are kept unchanged, the gradient shapes in the CHANGE intervals are optimized with a spline interpolation. This can be seen, for example, in the interval between the excitation pulse and the readout analog-to-digitial conversion (ADC). The zero-order gradient moment is kept unchanged, and the other boundary conditions like end and starting point are fulfilled. The spoiler after the readout as well as phase-

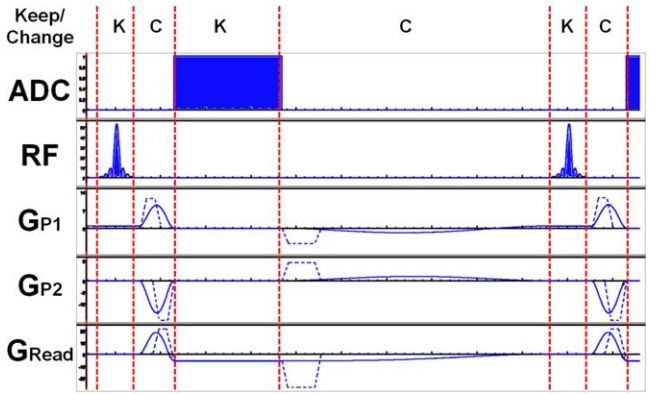

FIG. 2. Section of a sequence diagram of a clinical 3D GRE sequence. The nonoptimized original is shown by dashed lines and the algorithmically optimized adaption by solid lines. The KEEP and CHANGE intervals are indicated in the top row with K (KEEP) and C (CHANGE).

rewinding gradients are stretched as far as possible to enable strongly reduced slew rates.

Figure 3 shows in vivo images of the clinical T1 3D GRE protocol. Figure 3A corresponds to the original clinical sequence given above, and Figure 3B corresponds to the optimized sequence with identical protocol settings. For Figure 3C, a faster RF pulse was used to create more time to spread out the fast gradient pulses after the excitation. The measured acoustic noise levels were 89.0 dB(A) (Fig. 3A), 77.3 dB(A) (Fig. 3B), and 72.2 dB(A) (Fig. 3C), respectively. The CNRs between gray and white matter were 108 (Fig. 3A), 110 (Fig. 3B), and 108 (Fig. 3C), respectively. The image data were assessed by three radiologists for diagnostic content, image noise, and artifacts. No artifacts or differences in image quality were observed.

Figure 4 shows volunteer in vivo images acquired with the clinical T2 2D TSE protocol and optimizations given above. Using the optimized sequence with identical protocol parameters (Fig. 4B), acoustic noise decreased from 88.8 to 82.5 dB(A) compared with the nonoptimized sequence (Fig. 4A). By additionally increasing the echo spacing and the readout bandwidth, the acoustic noise could be reduced to 74.4 dB(A) (Fig. 4C). The CNRs between gray matter and cerebrospinal fluid are 289 (Fig. 4A), 284 (Fig. 4B), and 238 (Fig. 4C). The image data were analyzed by three radiologists for diagnostic content, image noise, and artifacts. No artifacts and no differences in image quality were observed due to the large CNR budget of the original image.

Figure 5 schematically explains the changes and the impact of the protocol changes on the gradients in readout and slice directions. The free induction decay spoiling moments stay constant, but gradient slew rates in this area can be decreased dramatically, as the spoiling moment fits into the ramp of the gradient pulse. Additionally, more time is available for the phase-encoding blips, and lower slew rates are also possible in the phase-encoding direction. Additionally, edges of the gradients are smoothed by the conversion algorithm.

The measured acoustic spectra of the T2 2D TSE sequences with and without optimization are compared in Figure 6. Note that the two scans have identical protocol settings.

DISCUSSION

In the example scans with algorithmically optimized gradients and identical protocol settings shown in Figures 3A and 3B and Figures 4A and 4B, the acoustic noise could be reduced by 11.7 dB(A) in the GRE scan and 6.3 dB(A) in the TSE scan, which corresponds to a reduction of sound pressure by 74% and 52%, respectively. Because all protocol parameters were kept constant, practically no changes were observed in image quality, and particularly CNR behavior.

In a second optimization step reflected by the results in Figure 3C and Figure 4C, we applied changes to the initial protocol to further reduce the slew rates. These protocol changes were chosen carefully in order not to change the contrast or diagnostic content of the images. Therefore, we limited changes of timing parameters to below 10%.

For GRE sequences, timing is critical due to the in-phase and opposed-phase conditions. Thus, in many protocols, echo times have to be kept constant. In order to create time for gradient ramps, we used an excitation pulse with higher bandwidth and a slightly increased readout bandwidth. For Figure 3C, an additional 5.1 dB(A) noise reduction compared with the algorithmically optimized unchanged protocol could be obtained. A total

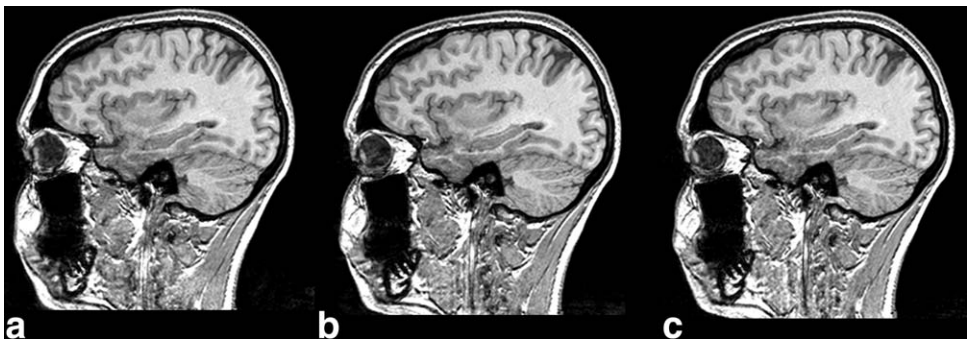

FIG. 3. T1-weighted 3D GRE volunteer images using (A) the clinical routine implementation, (B) the identical protocol with optimized gradients, and (C) an optimized sequence with slight protocol adaptions. Images have identical windowing. The acoustic noise levels are (A) 89.0 dB(A), (B) 77.3 dB(A), and (C) 72.2 dB(A).

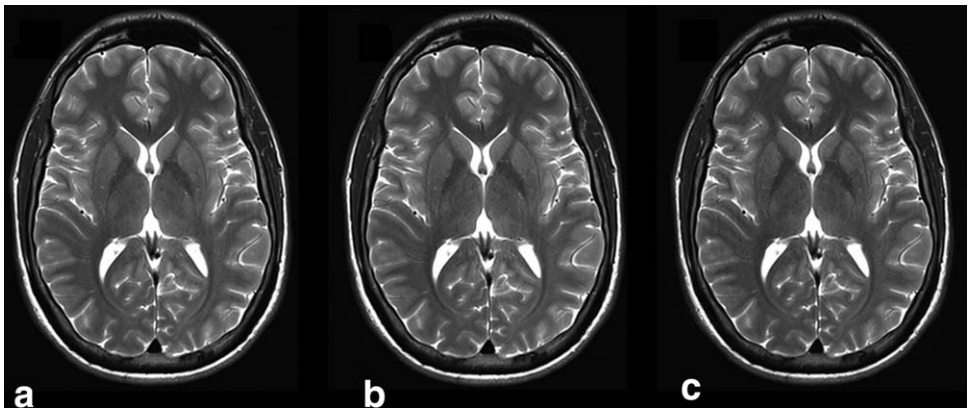

FIG. 4. T2-weighted 2D TSE volunteer images using (A) the clinical routine implementation, (B) the identical protocol with optimized gradients, and (C) an optimized sequence with slight protocol adaptions. Images have identical windowing. The measured acoustic noise levels are (A) 88.8 dB(A), (B) 82.5 dB(A), and (C) 74.4 dB(A).

acoustic noise reduction of 16.8 dB(A) is achieved in this case. This corresponds to a reduction of sound pressure by 86%.

For the TSE sequence results in Figures 4B and 4C, slew rates can be further lowered by using longer echo spacings and higher pulse or readout bandwidths. As in the GRE sequence, we limited the changes to specific protocol parameters to 10%. Acoustic noise could be reduced by another 8.1 dB(A) compared with the optimized sequence with unchanged protocol, resulting in a total noise reduction of 14.4 dB(A), which corresponds to a reduction of sound pressure by 81%.

From Figure 6, it can be seen that not only the absolute acoustic noise level, but also the characteristic of the acoustic noise spectrum changes. Due to the smoothing of gradients, high acoustic frequencies are minimized. This results in a deeper overall sound impression, which might additionally render the scan more comfortable for the patient.

Note that the standard clinical sequences also employ high slew rates to enable well-defined encoding and spoiling of spins in volumes affected by blood flow. As the sequence optimization algorithm reduces gradient slew rates resulting in longer encoding or spoiling times, differences in flow characteristics might occur in some cases. In the measured set of volunteer head examination images, no differences were observed.

In comparison to previously investigated sequence-based approaches, the algorithm does not require a manual adaption of the sequence, ensuring an automatic preservation of spin physics. The spline interpolation enables an optimized gradient curve regardless of timing constraints.

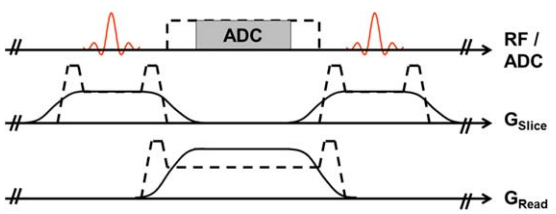

FIG. 5. Schematic diagram of the TSE sequence with original (dashed line) and slightly changed protocol (solid line). By increasing the readout bandwidth and keeping all other parameters constant, more time is generated for the free induction decay spoiler and the spoiling moments fit within the gradient ramps.

CONCLUSION

Acoustic noise in clinical MRI scans is mainly due to Lorentz forces on the gradient coil system. We implemented a general-purpose algorithm to optimize gradient slew rates holistically over the time course of an arbitrary MRI sequence. It automatically subdivided the time scheme of the sequence into KEEP and CHANGE intervals. KEEP intervals were marked by pulse, ADC, or flow compensation gradient activity; the intermittent time intervals were CHANGE intervals. Five boundary conditions preserving the continuity and slope of the gradient curves at the interval borders and the net spin phase changes were established. A fourth-order spline was used as a smooth substitution for gradient time curves in the CHANGE intervals. We applied the algorithm to typical clinical T1 3D GRE and T2 2D TSE sequences. Acoustic noise reductions of 11.7 dB(A) and 6.3 dB(A) were observed for the GRE and TSE sequences, respectively. Additional protocol optimizations yielded typical

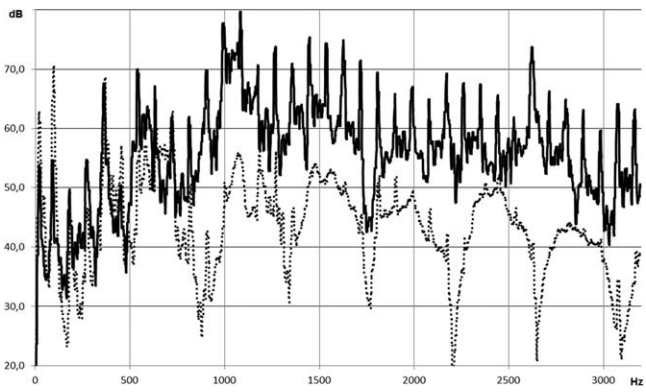

FIG. 6. Measured acoustic spectra without (solid line) and with (dashed line) optimization of the T2-weighted 2D TSE sequence from Figures 4A and 4B. All protocol parameters (TE, TR, resolution, etc.) were identical for both scans.

total acoustic noise reductions of 16.8 dB(A) and 14.4 dB(A), respectively. This corresponded to a reduction of sound pressure of 86% and 81%, respectively.

For the GRE image set, no relevant changes in CNR were observed, and no artifacts were encountered. The TSE images showed no visible degradation in CNR for the algorithmic optimization. The further protocol optimization reduced the CNR without affecting clinical diagnostic value. Note that specific sequences and protocols relying on maximum slew rates might not benefit from the approach to this high extent (e.g., EPI-based protocols and fast and high-resolution 2D GRE protocols with in-phase echoes at high field strengths). The results indicate that a substantial reduction of acoustic MRI noise by means of both generic algorithmic sequence optimization and careful protocol optimization can be achieved.

REFERENCES

1. McJury M, Shellock FG. Auditory noise associated with MR procedures: a review. J Magn Reson Imaging 2000;12:1:37–45.
2. Quirk ME, Letendre AJ, Ciottone RA, Lingley JF. Anxiety in patients undergoing MR imaging. Radiology 1989;170:2:463–466.
3. Mansfield P, Glover PM, Beaumont J. Sound generation in gradient coil structures for MRI. Magn Reson Med 1998;39:4:539–550.
4. Hedeen RA, Edelstein WA. Characterization and prediction of gradient acoustic noise in MR imagers. Magn Reson Med 1997;37:1:7–10.
5. Idiyatullin D, Corum C, Park JY, Garwood M. Fast and quiet MRI using a swept radiofrequency. J Magn Reson 2006;181:2:342–349.
6. Loenneker T, Hennel F, Ludwig U, Hennig J. Silent BOLD imaging. MAGMA 2001;13:2:76–81.
7. Hennel F. Fast spin echo and fast gradient echo MRI with low acoustic noise. J Magn Reson Imaging 2001;13:6:960–966.
8. Hennel F, Girard F, Loenneker T. "Silent" MRI with soft gradient pulses. Magn Reson Med 1999;42:1:6–10.
9. Schmitter S, Bock M. Acoustic noise-optimized VERSE pulses. Magn Reson Med 2010;64:5:1446–1452.
10. Blecher W. The Hilbert-Moore sequence: acoustic noise optimized MR imaging. University of Mannheim, Mannheim, Germany, Ph.D. thesis, 2008.
11. Schmitter S, Diesch E, Amann M, Kroll A, Moayer M, Schad LR. Silent echo-planar imaging for auditory FMRI. MAGMA 2008;21:5: 317–325.
12. Segbers M, Rizzo Sierra CV, Duifhuis H, Hoogduin JM. Shaping and timing gradient pulses to reduce MRI acoustic noise. Magn Reson Med 2010;64:2:546–553.
13. Edelstein WA, Hedeen RA, Mallozzi RP, El-Hamamsy SA, Ackermann RA, Havens TJ. Making MRI quieter. Magn Reson Imaging 2002;20:155–163.
14. Goldman AM, Gossman WE, Friedlander PC. Reduction of sound levels with antinoise in MR imaging. Radiology 1989;173:2:549–550.
15. McJury M, Stewart RW, Crawford D, Toma E. The use of active noise control (ANC) to reduce acoustic noise generated during MRI scanning: some initial results. Magn Reson Imaging 1997;15:3:319–322.
16. Vegh V, Tieng QM, Brereton IM, Galloway GJ. A wrapped edge transverse gradient coil design for increased gradient homogeneity. Concepts Magn. Reson 2009; 35B:139–152.
17. Grodzki DM, Jakob PM, Heismann B. Ultrashort echo time imaging using pointwise encoding time reduction with radial acquisition (PETRA). Magn Reson Med 2012;67:2:510–518.